Towards Verification of Unstructured-Grid Solvers

James L. Thomas, NASA Langley Research Center, Hampton VA 23681*

Boris Diskin, National Institute of Aerospace, Hampton, VA 23666†

Christopher L. Rumsey, NASA Langley Research Center, Hampton VA 23681‡

New methodology for verification of finite-volume computational methods using unstructured grids is presented. The discretization order properties are studied in computational windows, easily constructed within a collection of grids or a single grid. Tests are performed within each window and address a combination of problem-, solution-, and discretization/grid-related features affecting discretization error convergence. The windows can be adjusted to isolate particular elements of the computational scheme, such as the interior discretization, the boundary discretization, or singularities. Studies can use traditional grid-refinement computations within a fixed window or downscaling, a recently-introduced technique in which computations are made within windows contracting toward a focal point of interest. Grids within the windows are constrained to be consistently refined, allowing a meaningful assessment of asymptotic error convergence on unstructured grids. Demonstrations of the method are shown, including a comparative accuracy assessment of commonly used schemes on general mixed grids and the identification of local accuracy deterioration at boundary intersections. Recommendations to enable attainment of design-order discretization errors for large-scale computational simulations are given.

*Senior Research Scientist, Computational Aerosciences Branch, Mail Stop 128, Fellow AIAA, James.L.Thomas@nasa.gov.

†Senior Research Scientist, 100 Exploration Way, bdiskin@nianet.org; Visiting Associate Professor, Mechanical and Aerospace Engineering Department, University of Virginia, Charlottesville. This research was supported by the National Institute of Aerospace under NASA Fundamental Aeronautics Program through NRA Contract NNL07AA23C and Cooperative Agreement NCC1–02043.

‡Senior Research Scientist, Computational Aerosciences Branch, Mail Stop 128, Associate Fellow AIAA, c.l.rumsey@nasa.gov.

Introduction

There is an increasing reliance on computational simulations in aircraft design practices, supplementing traditional analytic and experimental approaches. Verification and validation methodologies[1] are being developed to ensure the correct application of these simulations. Verification methodologies for structured grids are relatively well-developed in comparison to unstructured grids, especially grids containing mixed elements or grids derived through agglomeration techniques. The summary of the latest of three Drag Prediction Workshops[2] illustrates the problems associated with assessing errors in practical complex-geometry/complex-physics applications. Current practices tend to compare relative errors between methods and experimental results rather than absolute errors. The motivation for this paper was to advance verification methodologies to predict the code performance in such large-scale computational endeavors.

The verification methodologies proposed here stem from a novel *computational* tool, a *downscaling (DS) test*, for evaluating the accuracy of finite-volume discretization (FVD) schemes defined on general unstructured meshes.[3] Performed for a known exact or manufactured solution, the test consists of a series of inexpensive computational experiments that provide local estimates for the convergence orders of the discrete solution (discretization) errors by comparing errors obtained on different scales. The test does not impose any restriction on the grid structure. Analysis methods predicting the performance of DS tests were also developed. The downscaling technique is similar in motivation to the shrinking-grid method of Herbert and Luke[4] but is quite different near the boundaries and does not invoke statistically sampled results.

Traditionally, the discretization accuracy of FVD schemes has been verified by convergence of truncation errors (residuals evaluated with the exact solution). On irregular (unstructured) grids, the DS tests demonstrated, and global grid-refinement computations confirmed, that the discretization accuracy is not directly linked to convergence of truncation errors. In fact, many researchers have observed that convergence of truncation errors is a sufficient but not a necessary condition.[5–8] As such, from the standpoint of verification, truncation error convergence provides a conservative estimate of discretization error convergence.

The main contribution of the current paper is the use of computational windows to improve verification of unstructured-grid computational methods intended for large-scale applications. In large-scale grid-refinement studies, extensive amounts of data are involved and integral norms often do not provide sufficient information to isolate the source of errors. As an alternative, convergence of discretization errors is studied within computational windows, constructed within a collection of grids or a single grid. The concept of consistent refinement is introduced to allow a meaningful assessment of asymptotic error convergence on unstructured grids. A test performed in each window addresses a combination of problem-, solution-, and discretization/grid-related features affecting discretization error convergence. The windows can be adjusted to isolate par-

ticular elements of the computational scheme, such as the interior discretization, the boundary discretization, or singularities, or tailored to pinpoint regions of interest. Testing can use traditional grid-refinement computations within a fixed window or downscaling, using computations within windows contracting toward a focal point of interest. Also, in DS-testing, very small mesh sizes can be used to ensure that testing is within the asymptotic convergence range (where the leading-order terms dominate).

Verification method	Complexity	Interpretation
Grid-refinement computations of discretization errors	expensive	precise estimate
DS computations of discretization errors	fixed cost	optimistic estimate
Truncation errors via grid-refinement or DS computations	low	conservative estimate

Table 1. Verification methodologies.

The possible methodologies for verifying convergence of discretization errors on unstructured grids are listed in Table 1. The entries in the table are arranged from highest to lowest computational cost. Unfortunately, the less expensive estimates are more difficult to interpret correctly. For example, large-scale 3D grid-refinement computations are quite expensive; but it is quite simple to ascertain attainment of design order in grid refinement if an exact solution is available. DS computations keep the computational costs tractable by reducing the physical size of the domain with succeeding computations, but the DS tests can be overly optimistic in predicting global discretization-error convergence because they do not account for possible error accumulation. For unstructured grids, our experience has been that DS-test predictions of discretization accuracy have been the same as grid-refinement predictions. In any case, because DS tests are always optimistic predictors of discretization error convergence, if a DS test fails to demonstrate the design performance, there is certainly a deficiency in either the formulation or the implementation. In monitoring truncation errors, the solutions need not be determined, only residuals need to be evaluated with the manufactured solution. Because this is a local evaluation, there is little difference in convergence orders of truncation errors between grid-refinement and DS tests. Truncation error assessment is thus inexpensive, but it can serve only as an upper bound, often overly conservative, on discretization error convergence. This hierarchy of verification tools can be used to complement current practices in large-scale simulations.

The paper is organized as follows. Relations between truncation and discretization errors are discussed first, followed by the definition of consistent refinement with an example. Windowing and downscaling are discussed in the next two sections. Examples are shown for elliptic and in-

viscid equations, including a comparative accuracy assessment of commonly used FVD schemes on general unstructured grids of mixed type and local accuracy deterioration at boundary intersections using tailored DS tests. Recommendations on verification procedures intended for use within large-scale computational applications are given. The final section contains concluding remarks.

Discretization and Truncation Errors

The FVD schemes are derived from the integral form of a conservation law,

$$\oint_{\Gamma} (\mathbf{F} \cdot \hat{\mathbf{n}})\, d\Gamma = \iint_{V} (f - S)\, dV, \tag{1}$$

where f is a forcing function independent of the solution, S is a solution-dependent source function, V is a control volume with boundary Γ, $\hat{\mathbf{n}}$ is the outward unit normal vector, and $\mathbf{F}$ is the flux vector. The main accuracy measure of any FVD scheme is the *discretization error*, E_d, defined as the difference between the exact continuous solution, Q, to the differential conservation law

$$\nabla \mathbf{F} = f - S \tag{2}$$

and the exact discrete solution, Q^h, of the discretized equations (1)

$$E_d = Q - Q^h. \tag{3}$$

A scheme is considered as design-order accurate, if its discretization errors converge with the design order in the norm of interest.

A common approach to evaluate the accuracy of discrete schemes is to monitor the convergence of *truncation errors*. Traditionally, truncation error, E_t, measures the accuracy of the discrete approximation to the differential equations (2).[9,10] For finite differences, it is found by computing the discrete residuals after substituting the exact solution for the discrete solution. For FVD schemes, the traditional truncation error is usually defined from a time-dependent standpoint.[11,12] In the steady-state limit, after substituting the exact solution Q into the normalized discrete equations (1), the truncation error is defined as

$$E_t = \frac{1}{|V|} \left[\iint_{V} \left(f^h - S^h (Q) \right) dV - \oint_{\Gamma} \left(\mathbf{F^h} (Q) \cdot \hat{\mathbf{n}} \right) d\Gamma \right], \tag{4}$$

where $\mathbf{F^h}$ is a reconstruction of the flux $\mathbf{F}$ at the boundary Γ, $|V|$ is the measure of the control volume,

$$|V| = \iiint_V dV, \tag{5}$$

f^h and S^h are, respectively, approximations of the forcing function f and the source function S on V, and the integrals are computed according to some quadrature formulas.

Assuming the discretization error is small compared to the exact solution, Q, ($|E_d| << |Q|$), the discretization error can be evaluated as

$$E_d \approx J^{-1}(Q) E_t(Q), \tag{6}$$

where

$$J\left(Q\right) = \frac{\partial}{\partial Q} E_t(Q) \tag{7}$$

is the Jacobian of the truncation error expression (4).

The traditional definition of truncation error is very useful for structured (regular) grids because the truncation errors converge as $O(h^p)$ on sequences of refined meshes, where h is a characteristic mesh size and p is the design discretization-accuracy order of the method. For unstructured grid computations, the convergence of traditional truncation errors is often misleading. Previous studies[6,13–15] noted that 2nd-order convergence of truncation errors for some commonly used FVD schemes can be achieved only on grids with a certain degree of geometric regularity. Examples published elsewhere[3,5–8] and in this paper show that the truncation errors of a design-order scheme can exhibit a lower order of convergence or, in some cases, not converge at all. For some formally inconsistent FVD schemes (traditional truncation errors do not converge), it has been rigorously proven that the discretization errors, in fact, converge.[8]

The relation (6) provides the correct order of discretization-error convergence given the truncation error convergence order. The complexity of evaluation of the discretization-accuracy order rests with evaluation of the inverse Jacobian; as mentioned above, truncation errors are easy to compute for a representative manufactured solution. The inverse Jacobian accounts for both interior and boundary discretizations. An example of evaluations of the inverse Jacobian for a formulation focusing on the discrete boundary conditions is given elsewhere.[16] An approximate solution of (6) using an equivalent linear operator approach has been used to improve the understanding of relations between truncation and discretization errors.[3] Although the approach neglects error accumulation mechanisms, it can distinguish clearly between inviscid and viscous equations and even between different equations/solution components within a given system.

In this paper, tests are performed for representative manufactured solutions. The manufactured solutions used herein are of two types, either simple analytic functions (collections of polynomials or sines) or exact solutions. The corresponding forcing functions are found by substituting these solutions into the continuous governing equations and boundary conditions. The intent of the

approach is to facilitate testing of discretizations and boundary conditions *in situ* for large-scale computations; this is possible with slight modifications of most boundary conditions, e.g., evaluating no-slip conditions with a specified wall velocity instead of the typical zero velocity condition. Likewise, in the farfield, the exterior conditions are taken from the exact solution rather than from the typical assumption of constant exterior conditions. Not all boundary conditions are amenable to such modifications (e.g., inviscid tangency) and for these we use exact (or manufactured) solutions associated with a particular geometry. An alternative is the mapping construction used by Bond et al.[17]

Consistent Refinement

The general FVD approach requires partitioning the domain into a set of non-overlapping control volumes and numerically implementing equation (1) over each control volume. Two types of FVD schemes are considered: node-centered schemes, in which solution values are defined at the mesh nodes, and cell-centered schemes, in which solutions are defined at the centroids of the control volumes. In the 2D examples considered here, the primal meshes are composed of triangular and quadrilateral cells; in 3D computations the cells are tetrahedral, prismatic, or hexahedral. The *median-dual* partition[18,19] used to generate control volumes for the node-centered discretization is illustrated in Figure 1 for two dimensions. These non-overlapping control volumes cover the entire computational domain and compose a mesh that is dual to the primal mesh. For cell-centered FVD schemes, the primal cells serve as control volumes (Figure 1).

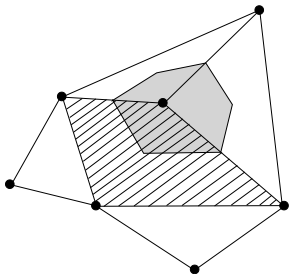

Figure 1. Illustration of node-centered median-dual control volume (shaded) and cell-centered primal control volume (hashed) in FVD schemes.

The discrete solution is represented as a piecewise linear function defined either within primal or dual cells. The discretizations are applied on a sequence of refined grids satisfying the *consistent refinement property*. For global grid refinement, this property requires the characteristic distance across primal and dual cells to decrease consistently with increase of the total number of degrees of freedom, *N*. The characteristic distance should tend to zero as $N^{-1/d}$ where d is the number of spatial dimensions. The property enables a meaningful assessment of the asymptotic order of error convergence. In particular, on 3D unstructured meshes satisfying the consistent refinement property, the discretization errors of 2$^{\text{nd}}$-order FVD schemes are expected to be proportional to $N^{-2/3}$.

An equivalent mesh size based on the degrees of freedom is defined as $h_N = N^{-1/d}$. An equivalent mesh size based on a characteristic distance is defined in terms of norms of the local

control-volume function, i.e., $h_V = ||V^{1/d}||$ where $||\cdot||$ is a norm of choice. For consistently refined meshes, h_V is a linear function of h_N for any computational subdomain (or the entire domain). The assessment of consistent refinement is purely geometric and could be done automatically by inspecting the meshes over local subsets of the domain. Such a technique is envisioned to be most useful during the grid generation phase to identify and repair regions where the grids are not consistently refined.

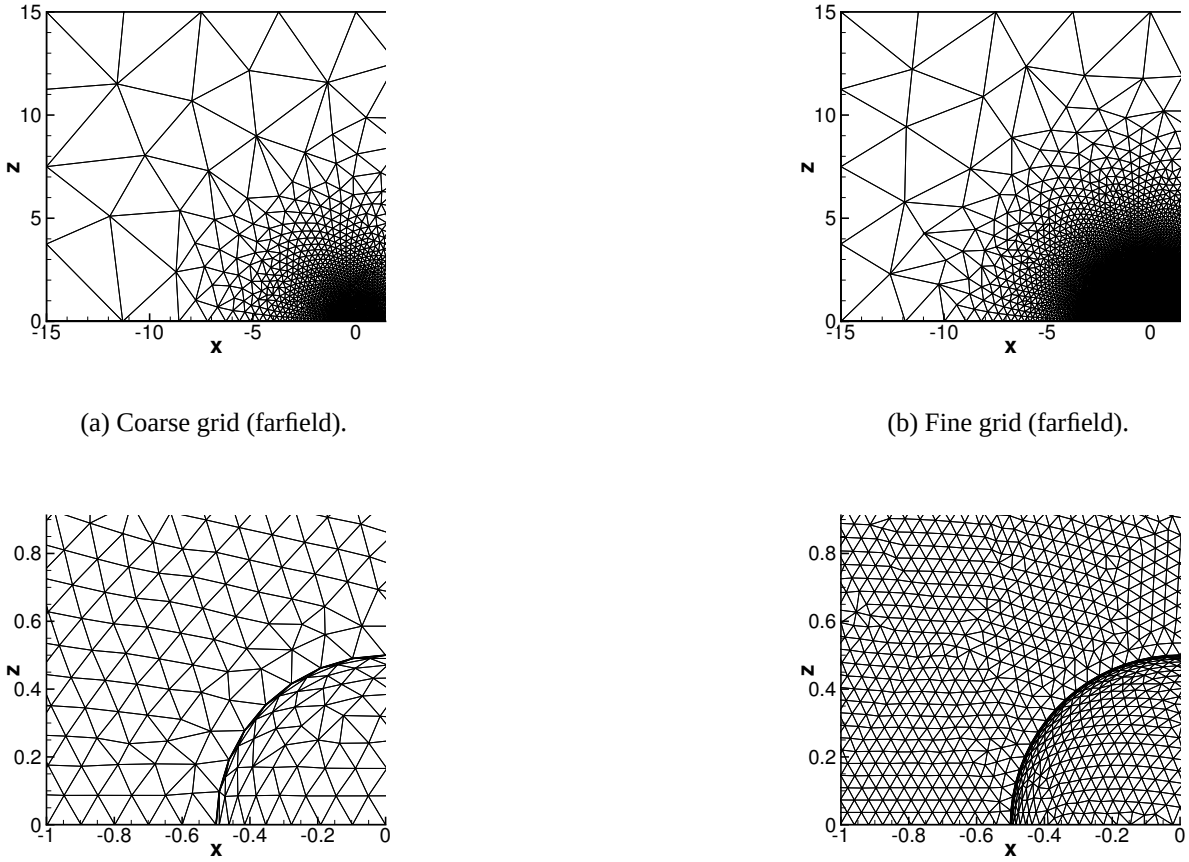

(a) Coarse grid (farfield).

(b) Fine grid (farfield).

(c) Coarse grid (nearfield).

(d) Fine grid (nearfield).

Figure 2. Partial view of surface grids on symmetry plane and sphere.

To illustrate the concept, we analyze three unstructured tetrahedral grids generated around a sphere; the grids are composed of 25,473 nodes, 82,290 nodes, and 328,463 nodes. In Figure 2, farfield and nearfield views of the coarsest and finest surface grids are shown. In Figure 3, variations of h_V based on the L_1 and L_∞ norms of $V^{1/3}$ are shown versus the equivalent mesh size $h_N = N^{-1/3}$, each normalized by the value on the coarsest grid. A consistently refined mesh variation is denoted by a dashed line in the figure. Based on the L_1 norm, h_V is linear but the h_V computed with the L_∞ norm shows that the mesh is not consistently refined. Examination of the grids in Figure 2 confirms that the mesh near the farfield boundary is not consistently re-

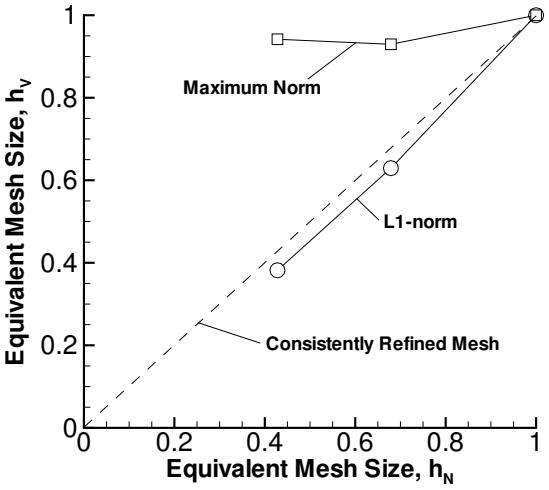

Figure 3. Consistent refinement check using normalized equivalent mesh sizes.

fined. Inviscid incompressible equations for the flow around a sphere have been discretized with a 2nd-order node-centered FVD scheme and solved on these grids. The L_1 norms of the errors in pressure over the field, shown versus h_V in Figure 4, converge with second order, in spite of the inconsistent refinement. This result is attributed to solution variations being much larger near the surface than near the farfield boundary. Although not shown, we performed computations in a window restricted to a region near the outer boundary and verified that the discretization error convergence order degrades.

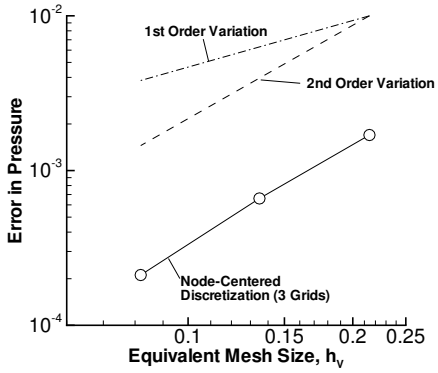

Figure 4. Variation of L_1 norm of error in pressure over the field with grid refinement.

Windowing

To provide a framework for assessing performance of codes in specific large-scale computations, we introduce the concept of windowing. A window is an arbitrarily-shaped subdomain

within the computational domain serving as a reference frame for testing and usually contains a focal point of interest. Figure 5 shows a sketch of possible windows superimposed on an unstructured grid. Solid line regions are shown with black focal points and dashed-line regions are shown with gray focal points; the latter regions preserve the body geometry (curvature) within the windows. Each test captures an entry from the three groups of features affecting error convergence: (1) problem-related features; (2) solution-related features; and (3) discretization/grid-related features.

The problem-related features are determined by the scope of required computations. Specifically, the features include the interior governing equations, various types of boundary conditions (e.g., inflow, outflow, tangency, no-slip, symmetry), and the geometrical features characterizing boundaries (e.g., flat boundary, curved boundary, sharp corners). To address the problem-related features, the windows should be placed in representative locations (interior, boundaries, corners, etc.).

The solution-related features account for variations in the solutions typically encountered, including smooth flows, shocks, stagnation regions, vortices, boundary layers, recirculating flows, etc. Each feature should be represented by a specific choice of the manufactured solution.

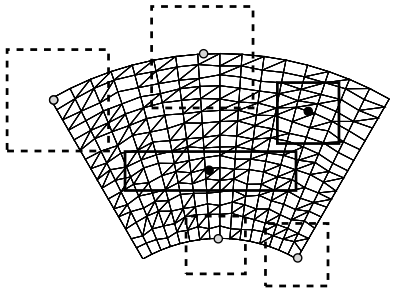

Figure 5. Sketch of possible windows superimposed on an unstructured grid. Regions denoted by dashed line are windows preserving body geometry (with gray focal points).

The discretization/grid-related features concern variations in meshes and discretization schemes. The features include the interior discretization scheme, discretization of boundary conditions, grid composition (e.g., combinations of advanced-layer (prismatic) regions with interior tetrahedral regions), approximation of geometry (flat panel or higher-order approximation), etc. Interfaces between regions with different types of meshes as well as allowed grid singularities, such as hanging nodes, degenerate cells, etc., should be considered as separate grid-related features.

Within computational windows, the FVD scheme under study is supplemented with a set of boundary conditions at the interface between the interior and the windowing domain (see white squares in Figure 6); overspecification from the known manufactured solution is a typical choice. If the computational window is bounded by a physical boundary, the physical conditions are implemented at the boundary surface; overspecification can still be applied at the remaining interfaces (see sketches of downscaled windows in Figure 6 and boundary tests in Figure 11). The freedom to choose the manufactured solution, the shape and size of the window, and the type of interface boundary conditions greatly simplifies testing. To verify a code for particular applications, each representative triplet of features requires a designated test; convergence of discretization errors

observed in all representative tests should be understood and accepted as satisfactory.

Downscaling (DS) Test

Establishing the discretization-error convergence order in global grid-refinement computations is often not practical because discrete solutions must be computed on grids with prohibitively many degrees of freedom. Constraining the computations to smaller windows makes them more affordable; the DS tests radically reduce the complexity by shrinking domains on grids with smaller meshsizes, so the number of degrees of freedom on each grid is kept (approximately) constant. Specifically, the DS test employs numerical computations on a sequence of contracted domains zooming toward a focal point within the original computational domain (Figure 6).

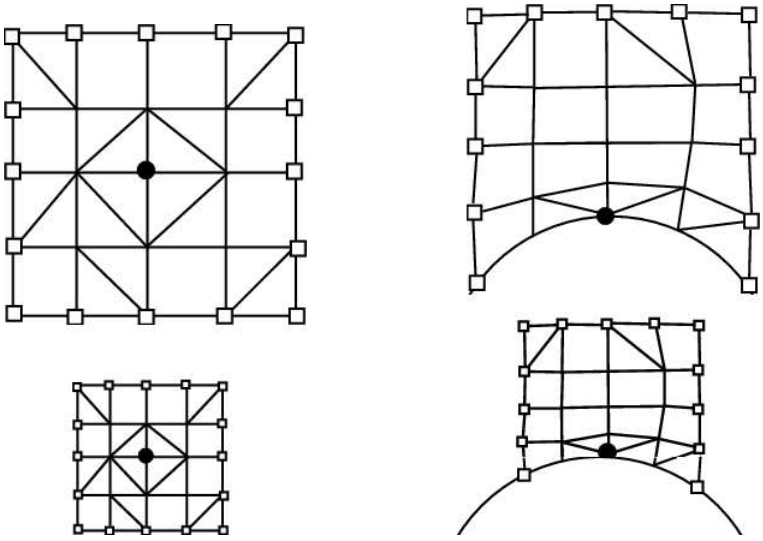

(a) Scaled grid.

(b) Independent grid generation (accounting for curved physical boundary).

Figure 6. Illustration of DS computational domains. Black bullets mark the focal points; white squares mark the interface between the interior and the DS-test domain.

There are at least two possible strategies for grid generation on these contracted domains. The first strategy is termed "scaled grid" (Figure 6(a)). With this strategy, the first (coarsest) computational domain is defined as a subdomain of the investigated global mesh containing the focal point; other (finer) domains and their mesh patterns are derived by scaling down this first domain (e.g., repeatedly multiplying all the distances from the focal point by a given factor, say, $1/2$ or $1/4$). The scaled-grid approach is especially useful for studying interior discretizations and straight boundaries. It is impractical for studies near a general (discretely defined) curvilinear boundary because the physical boundary shape should be preserved on each grid in the DS sequence. To overcome this limitation, an independent grid (Figure 6(b)) can be generated on each domain, assuming a modified consistent refinement property is satisfied, i.e., the characteristic distance across a grid cell is scaled down with the same rate as the diameter of the contracted domains. This second strategy is termed "independent grid generation."

The DS test evaluates local discretization-error convergence orders by comparing errors obtained in computations on different scales. The tests are performed in all representative compu-

tational windows for all representative triplet of features as described in the Windowing section. The convergence of errors in the L_∞ norm observed in global grid-refinement computations will be bounded by the worst DS-test estimate. Global convergence in integral norms, e.g., L_1 norm, may be better than the worst-DS estimate because these norms are less sensitive to fluctuations occurring locally.

One should interpret the DS test results carefully because they do not account for possible global discretization-error accumulation. In particular, on structured (regular) grids, convergence of discretization errors observed in DS tests is expected to be higher order than that observed in grid-refinement computations. In our experience, DS-test estimates of the discretization-error convergence orders on all truly unstructured multidimensional grids (meaning grids with little or no geometric regularity) have been sharp predictors of convergence observed in grid-refinement tests.

In any case, as mentioned earlier, if the convergence of discretization error observed in DS testing is slower than expected, this is an unambiguous indication of deficiencies in either formulation or implementation. Some deficiencies may be found acceptable, for example, when large discretization errors are generated locally and remain local, without affecting integral norms of the errors computed over the entire domain. As an example, for inviscid equations at stagnation, the convergence of discretization errors of velocity components tends to degenerate by one order.[3] This degeneration may or may not be noticed depending on the flow Reynolds number. Even if observed, the increased discretization error may stay local and not affect convergence of the L_1 norms of the discretization errors.

Example 1: Two-dimensional Laplace Equation

To illustrate applications of the verification methodology, we first consider the two-dimensional Laplace equation, as a model of the diffusion terms in the Navier-Stokes equations,

$$\Delta U = f, \tag{8}$$

subject to Dirichlet boundary conditions. The equations are discretized with a 2nd-order node-centered FVD scheme defined on a series of random mixed-element grids composed of triangles and quadrilaterals. The scheme is defined on median-dual control volumes and uses a combination of edge derivatives and Green-Gauss method for evaluating fluxes. Details of the discretization can be found elsewhere.[3,20] The manufactured solution and forcing term are taken as $U = [\sin^2(\pi x) + \sin^2(\pi y)]/2$, $f = -2\pi^2[1 - \cos^2(\pi x) - \cos^2(\pi y)]$.

For illustration purposes, the computations performed in windows contracted toward the center of the domain are compared with global grid-refinement computations. For global grid refinement,

each grid is formed from an underlying structured quadrilateral grid (Figure 7). In terms of a polar, (r, θ), coordinate system, the grid extent is defined as $\theta \in [\pi/3, 2\pi/3]$ in the circumferential direction and $r \in [1, 2.2]$ in the radial direction. The decision to split (or not to split) each structured quadrangle into triangles is determined randomly; approximately half of the quadrilaterals are split. In addition, the interior grid points are perturbed from their original position by random shifts in the range $[-\sqrt{2}/6,\ \sqrt{2}/6]$ of the local mesh size in the radial direction. The sequences of globally refined grids are generated with $2^{n+3} + 1$ points in both the radial and circumferential directions, where $n = 0,\ 1,\ 2,\ 3,\ 4$. The sequences of DS grids are generated from a grid with 17 points in both the nominal radial and circumferential directions and downscaled about the center of the domain, $r = 1.6, \theta = \pi/2$, by a factor 2^{-s}, where $s = 0,\ 2,\ 4,\ 6,\ 8$. The grid topology remains unchanged.

The L_1 norms of truncation and discretization errors are shown in Figure 8 versus an equivalent mesh size parameter, h_V. Although not shown, error convergence rates in the L_∞ norm are the same as the L_1-norm rates. In grid-refinement computations, the truncation errors remain $O(1)$ and the discretization errors converge with 2nd-order, precisely as predicted by the DS test. The reason for the $O(1)$ convergence of truncation errors is grid irregularity stemming from the usage of truly unstructured grids. As mentioned previously, the literature frequently associates $O(1)$ convergence of truncation errors on irregular grids as an indication of an inconsistent scheme that never converges to the exact result;[13,21] this example clearly shows design-order convergence of truncation errors is not a necessary condition.

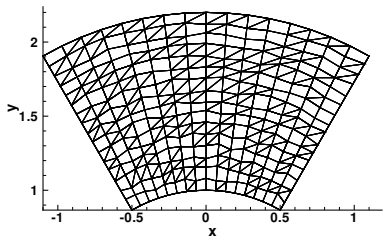

Figure 7. A typical mixed-element unstructured grid generated with random splitting and random perturbation of the underlying quadrilateral grid.

Example 2: Two-dimensional Incompressible Euler Equations

In this section, we consider incompressible inviscid equations in the interior and next to the curved tangency boundary. Inviscid fluxes for conservation of mass and momentum are defined as

$$\mathbf{F} = \mathbf{f}\bar{\mathbf{i}} + \mathbf{g}\bar{\mathbf{j}} = \begin{bmatrix} \beta u \\ u^2 + p \\ uv \end{bmatrix} \bar{\mathbf{i}} + \begin{bmatrix} \beta v \\ uv \\ v^2 + p \end{bmatrix} \bar{\mathbf{j}}, \tag{9}$$

where the vector of unknowns, $Q = [u, v, p]$, includes the Cartesian velocities and the pressure; β is an artificial compressibility parameter,[20] taken as $\beta = 1$ here.

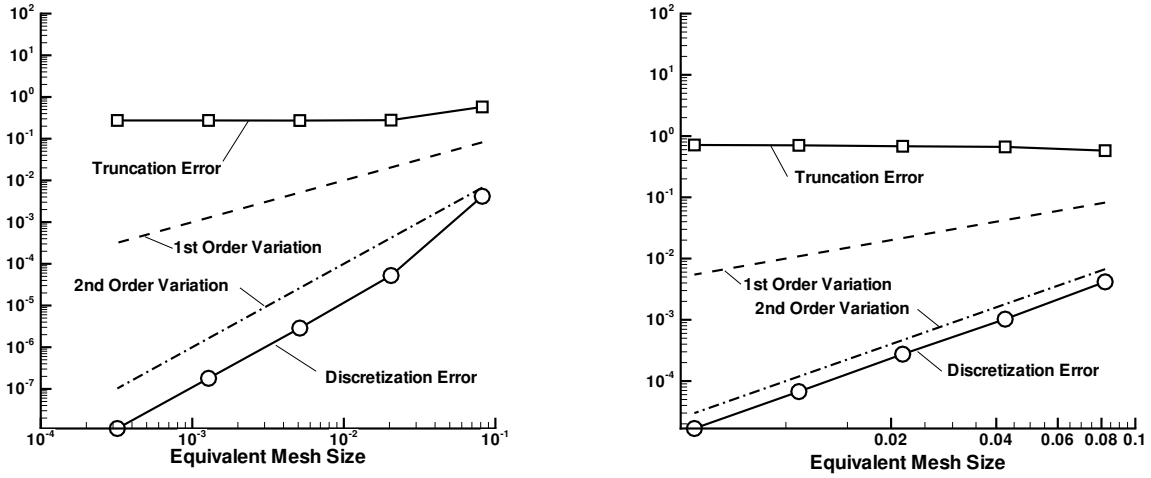

(a) DS test.

(b) Grid refinement test.

Figure 8. Convergence of the discretization and truncation errors for the Laplace equation solved on irregular mixed-element unstructured grids.

Two common FVD schemes with design 2$^{\text{nd}}$-order accuracy are investigated: an edge-reconstruction median-dual node-centered scheme and a cell-centered scheme. The node-centered FVD scheme uses the least-square method for gradient reconstruction and integration over the control-volume boundaries employing split (upwind) fluxes evaluated at the edge medians; details of the discretization can be found elsewhere.[3,20] The cell-centered FVD scheme also employs the least-square method for gradient reconstruction.[18] Numerical tests are performed for a non-lifting flow around a cylinder of unit radius centered at the origin. The analytical solution for this problem is well known.[3]

The first set of tests is performed to study accuracy of the interior discretization. The computational domain is shifted away from the surface of the cylinder: $1.5 \leq r \leq 4$, $2\pi/3 \leq \theta \leq 4\pi/3$. The two FVD schemes are studied on random triangular and random mixed-element grids. Examples of unstructured grids derived from an underlying structured grid are shown in Figure 9. Grid randomization is introduced through random splitting (or not splitting) of structured quadrilateral cells. Each cell has equal probabilities to introduce either of the two diagonal choices or, for mixed-element grids, no diagonals.

For each formulation, grid-refinement and DS tests are performed. In global grid-refinement computations, the underlying structured grid is refined by doubling the number of intervals in the radial and angular directions. Randomization is introduced independently on each scale. The inflow boundary conditions are enforced at the boundary corresponding to the external radius; outflow conditions are enforced at all other boundaries. In the DS test, the coarsest 9×9 grid is

scaled down around the point $r = 2.75,\ \theta = \pi$ by multiplying all angular and radial differences from this point by a factor of 0.5. Table 2 summarizes the convergence of discretization and truncation errors observed in these tests. The convergence orders are the same between DS and grid-refinement in all norms and for all variables and equations. The results are typical of our experience in comparing DS and grid-refinement tests for unstructured grids.

The observed discretization-error convergence rates indicate that the edge-reconstruction node-centered FVD scheme is 2nd-order accurate on triangular grids, but only first-order accurate on mixed-element grids; the cell-centered formulation is 2nd-order accurate on all studied grids. There are many ways to recover 2nd-order accuracy with the node-centered FVD scheme on mixed-element grids. For example, 2nd- and 3rd-order node-centered schemes have been demonstrated with face-reconstruction techniques for flux evaluation.[3]

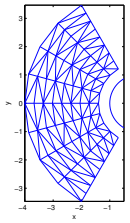

(a) Random triangular.

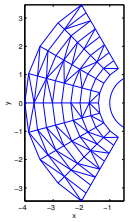

(b) Random mixed.

Figure 9. Typical unstructured grids for a computational domain shifted away from the surface of the cylinder.

For the edge-reconstruction node-centered scheme, we have also observed first-order convergence of discretization errors with randomly perturbed quadrilateral grids. The results are consistent with a previous publication[22] but contradict another.[13] In the latter reference, $O(1)$ convergence of discretization errors on randomly-perturbed quadrilateral grids with a central scheme was observed. Although not shown, we have implemented a central version of the edge-reconstruction node-centered scheme and tested it for various unstructured grids. We observed first-order convergence of discretization errors on mixed-element and random quadrilateral grids; an in-depth investigation of the discrepancies has been reported elsewhere.[3]

Another series of tests has been performed to study accuracy of the FVD schemes at the curved tangency boundary; both schemes use isotropic triangular grids approximating the curved tangency boundary by straight segments linking grid nodes located at the physical boundary. The approximation is illustrated in Figure 10 (a). The discrete tangency condition is enforced weakly over the straight segments.

A sequence of random triangular grids is generated at the top of the cylinder ($1 \leq r \leq 2.2$, $\pi/3 \leq \theta \leq 2\pi/3$); a grid example is shown in Figure 10 (b). Figure 11 illustrates convergence of the L_1 norm of truncation and discretization errors in DS tests performed with the node-centered edge-reconstruction FVD scheme. The left figure (a) exhibits convergence observed in the DS test with the focal point in the middle of the tangency boundary; the right figure (b) shows results for

Formulation	Downscaling computations		Grid-refinement computations	
	Trunc. Error	Discr. Error	Trunc. Error	Discr. Error
Node-centered, random triangular grid	$O(h)$	$O(h^2)$	$O(h)$	$O(h^2)$
Node-centered, mixed-element grid	$O(1)$	$O(h)$	$O(1)$	$O(h)$
Cell-centered, random triangular grid	$O(h)$	$O(h^2)$	$O(h)$	$O(h^2)$
Cell-centered, mixed-element grid	$O(h)$	$O(h^2)$	$O(h)$	$O(h^2)$

Table 2. Convergence of discretization and truncation errors for various unstructured grid formulations of the 2D inviscid incompressible equations on an inflow/outflow computational domain.

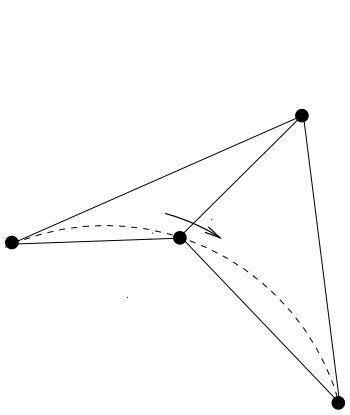

(a) Straight-segment approximations to curved tangency boundary (dashed line).

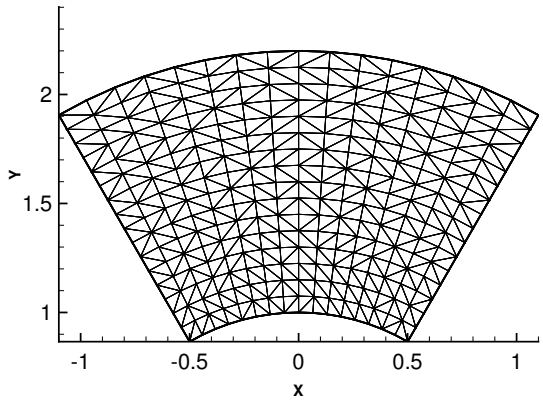

(b) Random triangular grid around the top of the cylinder.

Figure 10. Boundary approximation and grids for DS test of local boundary conditions.

the DS test with the focal point next to the inflow/tangency corner. See sketches in Figure 11, where the open squares denote boundaries with overspecification.

Convergence deterioration is clearly observed in the DS test performed with the inflow/tangency boundary conditions, indicating local loss of 2nd-order accuracy. This local accuracy deterioration is explained and repaired elsewhere.[3] Although not shown, the L_1 norms of the discretization errors in the corresponding grid-refinement test show the 2nd-order convergence, while the L_∞ norms of the errors converge with first order. These tests can serve as examples that local accuracy deterioration can be acceptable, if the cause and effect on discretization errors are fully understood. Analogous DS tests (not shown) performed for the cell-centered FVD scheme yielded 2nd-order

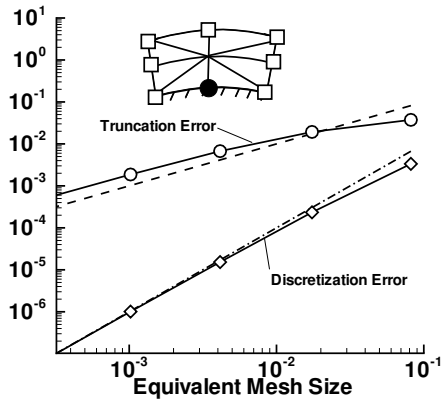

(a) DS test: interior tangency boundary condition.

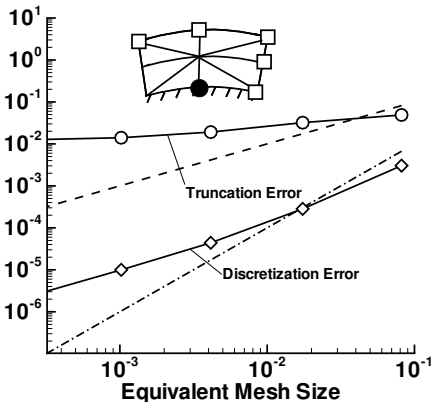

(b) DS test: inflow/tangency boundary conditions.

Figure 11. Convergence of the L_1 norm of $x-$momentum truncation errors and discretization errors in u observed in DS tests performed on random triangular grids surrounding the top tangency boundary of the unit cylinder; Dashed and dashed-dot lines denote 1st- and 2nd-order error variations; open squares in sketch denote boundaries with overspecification.

convergence of discretization errors at the interior tangency and at the inflow/tangency corner.

Example 3: Two-dimensional Compressible Euler Equations

In this section, we solve the compressible Euler equations for the flow over the smooth bump in a channel considered previously by Casper et. al.[23] Using a sheared Cartesian grid mapping, sequences of quadrilateral grids were generated. Mixed element grids were generated by randomly splitting half of the quadrilateral elements into two triangular elements; the mixed-element grid with 41 and 25 points in the longitudinal and vertical directions, respectively, is shown in Figure 12. Quadrilateral-element and mixed-element computations are shown for both node-centered and cell-centered formulations. Both formulations use a least-square method for gradient reconstruction and an approximate flux-difference-splitting scheme.

Tangency boundary conditions were applied on the upper and lower walls and freestream conditions corresponding to a Mach number of 0.3 were specified at the upstream and downstream locations. In this formulation, the approximate Riemann solver identifies appropriate inflow and outflow fluxes and a tare drag results, attributable to vorticity introduced at the upstream boundary. With an infinitely long channel, the tare drag asymptotes to zero.

Grid refinement computations are shown in Figure 13 of the drag minus the tare drag contribution of an infinitely refined mesh. The finest grid contained 641 and 385 points in the longitudinal and vertical directions, respectively. Both quadrilateral-element computations show a third-order variation in the integral measure of net drag. Although not shown, comparison of entropy errors,

similar to the technique used by Casper et. al,[23] verified the computations are second-order accurate. The mixed-element cell-centered computation is second-order accurate. The mixed-element node-centered computation is only first-order accurate because of the median-dual approximation of the flux. Windowing computations in the interior of the mesh, not shown, accurately predicted the lower-order behavior of the median-dual approximation for the node-centered mixed-element meshes.

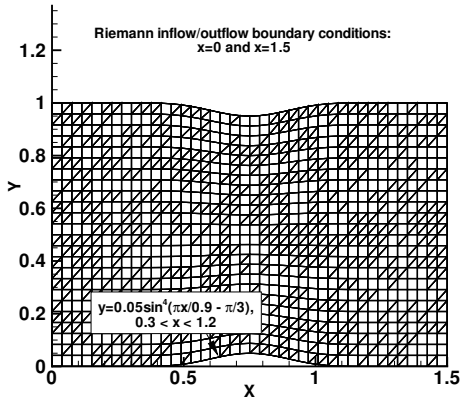

Figure 12. Mixed element grid for smooth bump in channel.

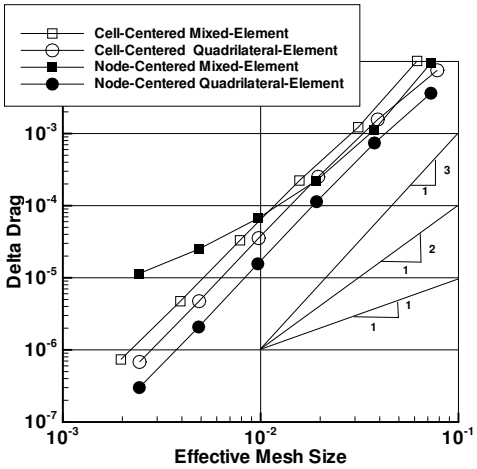

Figure 13. Comparison of drag variation with effective mesh size for quadrilateral and mixed-element grids for subsonic flow over smooth bump in channel.

Recommendations on Verification Procedure

In this section, we provide recommendations on choosing relevant tests to verify a code for a large-scale computation; the illustrative examples are motivated by the recent Drag Prediction

Workshops.[2]

There are two preliminary tests concerned with truncation-error computations (no need to compute discrete solutions), which are useful for confirming consistency of the investigated FVD scheme. The first test is performed for a smooth manufactured solution at fully-interior discretizations on *regular structured*, consistently-refined meshes; design-order convergence of truncation errors is expected. The second test is performed for a conservation law equation and a manufactured solution that produces linear fluxes: for example, mass conservation with constant density and linear velocity variations, or momentum conservation with constant density, constant velocity, and linear pressure variations. Second (or higher) order FVD schemes are expected to exhibit zero truncation errors for equations associated with linear fluxes on *any* mesh.

Assuming the FVD scheme passed these consistency tests, the first step toward forming a library of tests is to formulate a list (as complete as possible) of relevant problem-, solution- and discretization/grid-related features. The following list has been compiled for a mixed-element unstructured-grid solver considered for computations of a viscous flow around an airfoil.

- *Problem-related features* include Navier-Stokes equations with a given set of parameters, such as Mach and Reynolds numbers; turbulence model; far-field, symmetry, and no-slip boundary conditions; straight or smoothly curved profiles for the far-field and symmetry boundaries, smooth and discontinuous boundary profiles for the airfoil surface. Each problem-related feature is addressed by choosing an appropriate computational window.

- *Solution-related features* include smooth flow, stagnation flow, vortex, shock, boundary layer, and flow separation. Various solution features are allowed to interact. Each solution-related feature is addressed by choosing an appropriate manufactured solution.

- *Discretization/grid-related features* include the interior FVD scheme, boundary discretization scheme, advanced-layer prismatic meshes within the boundary layers, and general tetrahedral meshes in the exterior. Interfaces between the regions with different meshing and mesh singularities should be considered as separate grid-related features. Each feature is addressed in testing by constructing the grid (grid-refinement generally requires additional grid generation whereas DS-test may not) and by applying appropriate discrete equations.

A designated test should be designed for each relevant triplet of features, one from each group. Not all triplets are relevant; for example, there is no need to test the combination of a far-field boundary and a boundary-layer solution.

As examples, let us consider the tests recommended for verifying the interior discrete viscous equations (problem-related feature) for smooth solutions away from stagnation (solution-related feature). A computational window is placed away from all physical boundaries and a representative smooth manufactured solution is chosen. In tests performed within this window, 2^{nd}-order

convergence of discretization errors is expected. At least four basic combinations of nonsingular meshes should be considered as grid-related features: (1) general prismatic meshes, (2) general tetrahedral meshes, (3) random mixed-element meshes, and (4) meshes with a smooth interface between the prismatic and tetrahedral regions. If certain mesh singularities (e.g., hanging nodes, zero-volume elements, other types of elements beside triangular prisms and tetrahedrons) are allowed, they should be considered in separate tests, usually in combination with the four basic nonsingular meshes.

For verifying the formulation for smooth solutions in the vicinity of a smooth surface, one has to place the window at the surface and perform tests with general prismatic meshes and manufactured solutions representing boundary-layer flow, stagnation flow, and separated flow. For testing smooth solutions around sharply angled parts of the airfoil surface, the same manufactured solutions should be tested on general mixed-element meshes. We have explored only a subset of the recommended practices to date. In particular, the expected asymptotic behavior for discontinuous solutions has yet to be addressed.

Concluding Remarks

New methodology for verification of finite-volume computational methods using unstructured grids has been presented. The discretization order properties are studied within computational windows and address a combination of problem-, solution-, and discretization/grid-related features affecting discretization error convergence. The windows can be adjusted to isolate particular elements of the computational scheme or tailored to pinpoint regions of interest. Studies can use traditional grid-refinement computations within a fixed window or downscaling, in which computations are made within windows contracting toward a focal point of interest. The only constraint on the grids is that of consistent refinement, enabling a meaningful assessment of asymptotic error convergence on unstructured grids. This concept can be applied to assess families of mapped (block-structured) grids as well. Demonstrations of the method have been shown, including a comparative accuracy assessment of commonly used schemes on general mixed grids and the identification of local accuracy deterioration at boundary intersections. Recommendations to enable attainment of design-order discretization errors for large-scale computational simulations have been given. Perhaps the biggest roadblock to wider usage is that the complete process requires manufactured solutions appropriate to the application and such manufactured solutions are not widely available.

The second possible usage of the accuracy assessment methodology proposed in this paper is in the development of algorithms. Because developments are usually performed in a small-scale environment, demonstrations are simpler than large-scale applications and testing can use both downscaling and grid-refinement approaches relatively easily. Also, appropriate manufac-

tured solutions are easier to construct. Oftentimes improvements are needed to overcome observed shortcomings of a given scheme and the methodology can be used to pinpoint deficiencies and demonstrate improved capability. A build-up procedure can be used to verify elements of a proposed scheme in a methodical fashion, from interior residual discretizations to boundary residuals. Although we do not emphasize it here, we have found the overall process useful in developing efficient solvers, as well as discretizations, for unstructured grid schemes.

Acknowledgments

The three-dimensional results presented were computed within the FUN3D suite of codes at NASA Langley Research Center (`http://fun3d.larc.nasa.gov/`). The contributions of E. J. Nielsen and J. A. White of NASA in the implementation of the cell-centered discretization within FUN3D are gratefully acknowledged. The authors also thank the reviewers for their constructive comments and suggestions.

References

[1]Roache, P. J., Verification and Validation in Computational Science and Engineering, Hermosa, Albuquerque, NM, 1998.

[2]Morrison, J. and Hemsch, M., "Statistical Analysis of CFD Solutions from the Third AIAA Drag Prediction Workshop," AIAA Paper 2007-0254, January 2007.

[3]Diskin, B. and Thomas, J. L., "Accuracy Analysis for Mixed-Element Finite-Volume Discretization Schemes," NIA Technical Report 2007-8, August 2007.

[4]Herbert, S. and Luke, E. A., "Honey, I Shrunk the Grids! A New Approach to CFD Verification Studies," AIAA Paper 2005-685, January 2005.

[5]Manteuffel, T. A, and White, A. B. Jr., "The Numerical Solution of Second-Order Boundary Value Problems on Nonuniform Meshes," Mathematics of Computation, Vol. 47, No. 176, 1986, pp. 511-535.

[6]Giles, M. B., "Accuracy of Node Based Solutions on Irregular Meshes," Lecture Notes in Physics, Vol. 323, 1989, pp. 273-277.

[7]Aftosmis, M. J., and Berger, M. J., "Multilevel Error Estimation and Adaptive h-Refinement for Cartesian Meshes with Embedded Boundaries," AIAA Paper 2002-0863, Jan 2002.

[8]Despres, B., "Lax Theorem and Finite Volume Schemes, Mathematics of Computation, Vol. 73, No. 247, 2003, pp. 1203–1234.

[9]Tannehill, J. C., Anderson, D. A. and Pletcher, R. H., Computational Fluid Mechanics and Heat Transfer, 2nd Ed., Hemisphere, Washington, DC, 1997.

[10]Hirsch, C., Numerical Computation of Internal and External Flows Volume I : Fundamentals of Numerical Discretization, John Wiley & Sons, NY, 1988.

[11]Turkel, E., "Accuracy of Schemes with Nonuniform Meshes for Compressible Fluid Flows," Applied Numerical Mathematics, Vol. 2, 1986, pp. 529-550.

[12]Syrakos, A. and Goulas, A., "Estimate of the Truncation Error of Finite Volume Discretization of the Navier-Stokes Equations on Collocated Grids," Int. J. Numer. Meth. Fluids, Vol. 50, 2006, pp. 103-130.

[13]Svärd, M. and Nordström, J., "An Accuracy Evaluation of Unstructured Node-centered Finite-volume Methods," Applied Numerical Mathematics, Vol. 58, No. 8, 2008, pp. 1142-1158; also available as NIA Report 2005-04, NASA CR-2006-214293, April 2006.

[14]Roe, P. L., "Error Estimates for Cell-Vertex Solutions of the Compressible Euler Equations," ICASE Report 87-6, NASA CR-1987-178235, January 1987.

[15]Lindquist, D.R. and Giles, M. B., "A comparison of Numerical Schemes on Triangular and Quadrilateral Meshes," Lecture Notes in Physics, Vol. 323, 1989, pp. 369-373.

[16]Diskin, B, and Thomas, J. L., "Analysis of Boundary Conditions for Factorizable Discretizations of the Euler Equations," ICASE Report 2002-13, NASA CR-2002-211648, May 2002.

[17]Bond, R. B., Ober, C. C., Knupp, P. M., and Bova, S. W., "Manufactured Solutions for Computational Fluid Dynamics Boundary Condition Verification," AIAA Journal, Vol. 45, No. 9, September 2007, pp. 2224-2236.

[18]Barth, T. J., "Numerical Aspects of Computing High-Reynolds Number Flow on Unstructured Meshes," AIAA Paper 91-0721, January 1991.

[19]Haselbacher, A. C., A Grid-Transparent Numerical Method for Compressible Viscous Flow on Mixed Unstructured Meshes, PhD thesis, Loughborough University, 1999.

[20]Anderson, W. K. and Bonhaus, D. L., "An Implicit Upwind Algorithm for Computing Turbulent Flows on Unstructured Grids," Computers and Fluids, Vol. 23, 1994, pp. 1–21.

[21]Coirier, W. J., "An Adaptively-Refined, Cartesian, Cell-Based Scheme for the Euler and Navier-Stokes Equations," NASA TM-106754, October 1994.

[22]Aftosmis, M., Gaitonde, D., and Tavares, T. S., "Behavior of Linear Reconstruction Techniques on Unstructured Meshes," AIAA Journal, Vol. 33, No. 11, 1995, pp. 2038–2049.

[23]Casper, J., Shu, C.-W., and Atkins, H., "Comparison of Two Formulations for High-Order Accurate Essentially Nonoscillatory Schemes," AIAA Journal, Vol. 32, No. 10, 1994, pp. 1970-1977.